Observation and analysis of nonlinear scattering using the scattered-light imaging method

Kelly C. Jorge [1,*], Anderson M. Amaral [2], Albert S. Reyna [3], Leonardo de S. Menezes [4,2] and Cid B. de Araújo [2]

[1]*Instituto de Ciência e Tecnologia, Universidade Federal de São Paulo, 12.231-280, São José dos Campos, SP, Brazil*
[2]*Departamento de Física, Universidade Federal de Pernambuco, 50670-901 Recife, PE, Brazil*
[3]*Programa de Pós-Graduação em Engenharia Física, Universidade Federal Rural de Pernambuco,*
Unidade Acadêmica do Cabo de Santo Agostinho, 52171-900 Cabo de Santo Agostinho, PE, Brazil
[4]*Chair in Hybrid Nanosystems, Nanoinstitute Munich, Faculty of Physics,*
Ludwig-Maximilians-Universität München, D-80539 München, Germany

Optical phenomena like nonlinear absorption and nonlinear refraction are often determined through light transmittance techniques. However, in turbid or resonant media, scattering may also significantly attenuate the laser beam, such that absorptive losses may be overestimated. Thus, while transmittance techniques are suitable to determine the power extinction, it is often difficult to characterize the contribution of nonlinear scattering in a sample. In this work we applied the scattered-light imaging method to discriminate the nonlinear extinction due to nonlinear absorption and nonlinear scattering contributions in a turbid medium constituted of TiO_2 nanoparticles suspended in acetone. The single-shot method collects an image of the beam transverse profile evolution along the propagation axis inside the sample. It was observed that while the results obtained by the transmittance technique indicate the extinction coefficient (including scattering and absorption contributions), the results obtained with the scattered-light imaging method discriminate the contribution of each phenomenon. Therefore, the results of both approaches are complementary and allow a more complete characterization of turbid media.

I. INTRODUCTION

Light scattering is a phenomenon frequently observed in studies involving the propagation of electromagnetic waves in nonhomogeneous materials and rough surfaces. However, when light transmission based techniques are used to characterize the optical response of various systems, scattering is seldom the aspect of interest. Quite often, the scattering contributions are considered to play a minor role in absorption or extinction phenomena responsible for the intensity losses. Nevertheless, understanding the physical properties of light scattering can be used for example to characterize biological materials [1–3], nanoparticles [1,4], and laser beam profiles [5,6], or in techniques such as thermometry [7,8], random laser generation [9–11], and spatial solitons [12–15] among others.

In some applications, scattering can present nonlinear (NL) behavior due to distinct optical phenomena. In 1965, for the first time NL scattering was reported with the aim to study molecular structures and their interactions in liquids [16]. NL scattering is often considered as an inelastic process, where the scattered light is emitted with a frequency different from that of the incident light. A spectrum analyzer is often used as a detector to collect light scattered along forward, backward, or transverse directions. However, it is essential to note that it is also possible to have elastic NL scattering processes. NL scattering can occur in this regime when an intense laser

beam propagates in inhomogeneous media, such as colloids containing nanoparticles (NPs) suspended in a host medium, with different refractive indices [17]. For instance, consider a two-component colloid consisting of particles whose refractive index is $n_{particle}$ inside a solvent described by refractive index $n_{solvent}$ in the Rayleigh-Gans regime [18,19]. Then, the scattering cross section is proportional to $(n_{particle} - n_{solvent})^2$ and, if at least one material has a relevant Kerr response, then the scattering cross section becomes NL and may not involve changes in the photon frequency. Notice that this phenomenon can occur in general in samples where some constituent presents large NL polarizability.

The intensity dependence of scattering can produce substantial intensity losses along with the beam propagation [20], causing significant changes in other NL optical processes that can appear simultaneously, such as NL absorption and NL refraction. However, since the intensity losses by NL scattering exhibit a behavior similar to that induced by NL absorption, it is usual to observe the contributions of both NL phenomena included in a single process, known as NL extinction. The reason for commonly considering the combined effect of intensity losses lies in the simplicity of measuring the NL extinction coefficient α_{NL} [20] directly in a transmittance experiment using an optical detector. Nevertheless, although the NL extinction is sufficient to model NL extinction effects on propagating beams, the physical origins of the absorption and scattering phenomena are fundamentally different.

Traditionally, the Z-scan technique is widely used to characterize the effective NL absorption and refraction coefficients [21]. The Z-scan technique is based on measuring the

*kelly.sakamoto@unifesp.br

transmittance from the ratio between the output and input focused beam power in the sample while it is moved along the beam propagation direction (z axis), around the region with the highest intensity ($z = 0$). An aperture in front of a photodetector is used to define the closed-aperture (CA) and open-aperture (OA) schemes, used to measure NL refractive index and NL absorption coefficient, respectively [21,22].

In the OA Z-scan case, generally, it is assigned that the NL attenuation mechanism suffered by laser propagation in a sample is exclusively due to absorption. However, since Z-scan corresponds to a transmitted light detection technique, the NL absorption coefficient can be overestimated when the sample exhibits linear and/or NL scattering. Therefore, some strategies are implemented to the Z-scan technique to distinguish the contributions of NL absorption and NL scattering, such as spectral analysis of the transmitted light and the addition of new detectors to collect the output signal from different observation angles [17,23,24]. An alternative approach is to dilute the scattering material [25], therefore minimizing light scattering. There is also another version of Z-scan, which requires a more complex and expensive experimental setup [26].

The scattered-light imaging method (SLIM) is a versatile technique which was developed initially for laser beam characterization [5,6] in both continuous-wave and pulsed regimes. It has been shown to be an excellent tool to understand matter-light interactions. We can mention some applications of the SLIM, as the determination of the NL refractive index n_2 of scattering media [27], the characterization of solitons in cubic-quintc [14], quintic-septimal medium [13], and in saturable optical medium [15].

In comparison with SLIM, the Z-scan method presents a laborious experiment. It needs a large number of laser pulses during sample translation, while the SLIM requires a single image of a laser pulse to measure the same parameter with the sample fixed in one position. As a consequence, SLIM provides a measure that indicates the pulse-to-pulse beam point stability and intensity fluctuations.

In this work we use the SLIM [6] to measure the NL effects of turbid samples, discriminating the NL absorption and NL scattering contributions. The images obtained by using the SLIM allow us, in addition to visualizing the laser beam intensity profile as a function of the propagation distance, to measure the beam longitudinal power profile over the entire sample length. The NL scattering coefficient of a colloid, consisting of titania (TiO_2) NPs in acetone, was determined by fitting the beam longitudinal power profile with the theoretical model reported in [28]. The SLIM images presented here originated the development of this theoretical model [28], which discriminates between the responses due to NL scattering from the NL absorption. In addition, the OA Z-scan technique was used as a method to perform complementary extinction measurements.

II. EXPERIMENTAL SETUP

The experiments were done with three samples having different concentrations of TiO_2-NPs suspended in acetone (here indicated by **A**, **B**, and **C**). The samples were prepared by adding acetone in a water colloid containing spherical TiO_2-NPs with (168 ± 28) nm in diameter. The NPs number
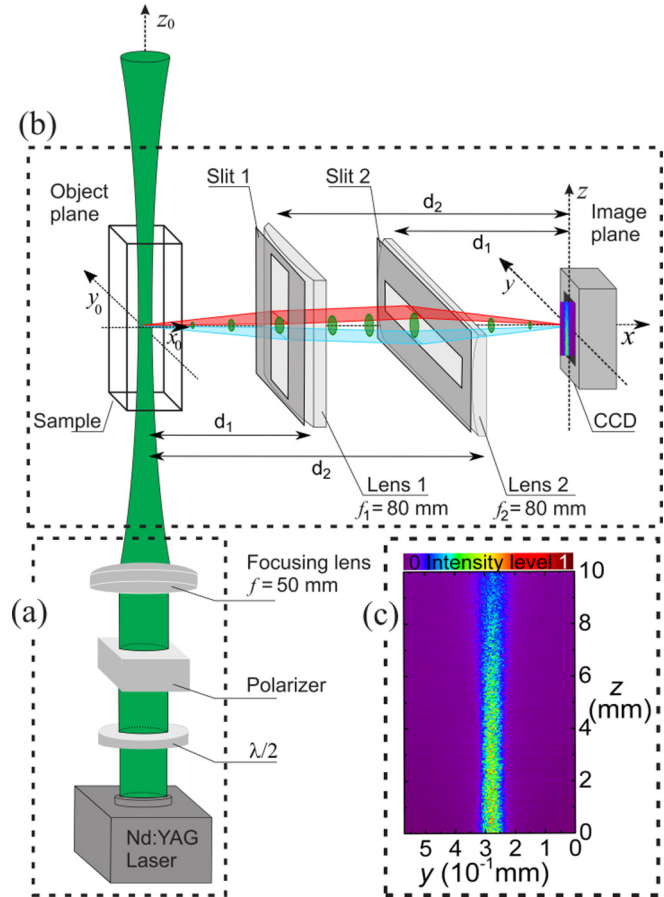

FIG. 1. SLIM experimental setup for characterizing turbid media. (a) Input laser beam irradiance control and focusing system. (b) Ray diagram for scattered light with $d_1 = 10.7$ cm and $d_2 = 21.3$ cm. (a) and (b) Adapted from [27]. (c) SLIM image of the laser beam propagation in sample **B** with $I_0 = 2.5$ GW/cm^2.

per volume was estimated by using the Rayleigh approximation [29] given by $N \cong \frac{3\alpha_1 \lambda^4}{128\pi^5 r^6 n_{\text{solvent}}^4} \left(\frac{m^2+2}{m^2-1} \right)^2$; considering the linear extinction coefficients (α_1) for $\lambda = 532$ nm that were determined through the curves of lower incident intensity using SLIM, shown in Table I in Sec. IV. r is the nanoparticles' radius (equal to 84 nm) and $m = \frac{n_{\text{NP}}}{n_{\text{solvent}}}$, with $n_{\text{NP}} = 2.6$ and $n_{\text{solvent}} = 1.36$ being the refractive index of the TiO_2 and acetone, respectively. The volume fractions were estimated by multiplying N times the volume of a nanoparticle ($\sim 2.48 \times 10^{-15}$ cm^3), resulting in 2.36×10^{-6} (**A**); 3.45×10^{-6} (**B**); and 5.23×10^{-6} (**C**), respectively.

Briefly, the SLIM setup is shown in Fig. 1(a), where the second harmonic of a Q-switched and mode-locked Nd:YAG laser, operating at 532 nm, with pulse duration of 100 ps and repetition rate of 10 Hz, was focused on a 10 mm quartz cell containing the sample. Five values of input beam irradiance (I_0) were used, varying from 2.5 to 12.5 GW/cm^2. Figure 1(b) shows an anamorphic imaging optical system, constituted of two cylindrical lenses (80 mm focal lengths) oriented perpendicularly to each other and a CCD camera, arranged orthogonally along one of the cell's side windows.

Figure 1(c) shows an image of the laser beam propagation inside sample **B** with low input irradiance ($I_0 = 2.5$
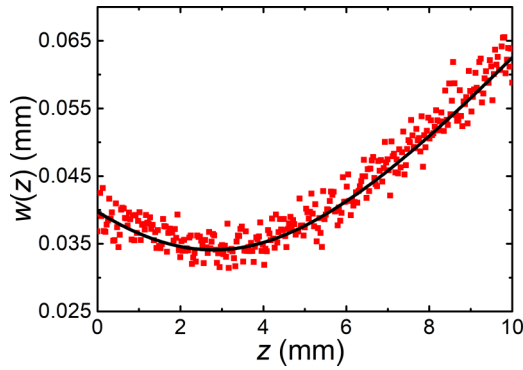
FIG. 2. Laser beam propagation curve of sample **B** (red solid squares) with input irradiance of 2.5 GW/cm^2. The fitted curve (black solid line) is given by $w(z) = \sqrt{0.034^2 + 10.1^2(z - 2.6)^2}$ in mm [30].

GW/cm^2), i.e., where the sample nonlinearity is negligible. Figure 2 shows the laser beam propagation curve fitted by $w(z)^2 = w_0^2 + \theta^2(z - z_0)^2$ [30], where its propagation parameters obtained in sample **B** were: the beam waist of $w_0 = (34.1 \pm 0.5)$ μm; the divergence of $\theta_0 = (10.1 \pm 0.2)$ mrad; the Rayleigh range of $z_R = (3.4 \pm 0.2)$ mm; and the quality factor of $M^2 = 2.71 \pm 0.01$. The beam waist position is located at $z_0 = (2.6 \pm 0.1)$ mm inside the cell that has 10 mm of length. Further details on the SLIM experimental setup are given in [6,27].

III. PROCESSING OF SLIM IMAGES

The optical axis of the imaging optical system is given on the x direction as shown in Fig. 1(b). In the object plane, the laser beam propagates along the z_0 axis, and the light of the beam is scattered in the $x_0 y_0$ plane. Notice that the imaging system cannot distinguish object features along x_0, such the image formed at the camera plane corresponds to the scattered intensity integrated along x_0 or $I(y_0, z_0) = \int I(x_0, y_0, z_0)dx_0$. The image formed at the camera's plane, $I(y, z)$, can therefore be used to determine the evolution of the beam intensity profile along the propagation direction. More details can be found in [6].

In order to determine the power of the laser beam propagating in the NL scattering medium as a function of the z position $P(z)$, the SLIM image $I(y, z)$ was integrated along the y direction:

$$P(z) = \int I(y, z)dy. \tag{1}$$

The natural logarithm of the beam power was calculated, and its processed data were fitted by using the theoretical model that describes the beam power evolution, within the sample, along a transverse direction to the beam propagation axis, which is detected by the SLIM scheme [28]:

$$\ln\langle P(z, t)\rangle = C + \ln I_0 - \alpha_1 z + \ln \Sigma_1$$
$$+ \ln\left[1 + \frac{\alpha_{2,S} I_0}{\alpha_{1,S}}\left(\frac{e^{-\alpha_1 z}}{1 + \Delta z^2/z_R^2}\right)\frac{\Sigma_2}{\Sigma_1}\right], \tag{2}$$

where C indicates the maximum linear detection efficiency of the system; $\Delta z = z - z_0$ is the distance relative to the beam waist position (z_0); z_R is the Rayleigh length; and α_1 and α_2 are the linear and NL extinction coefficients, respectively. The functions $\Sigma_1 = \sum_{i=0}^{\infty}\frac{[-A(z)]^i}{\sqrt{i+1}}$ and $\Sigma_2 = \sum_{i=0}^{\infty}\frac{(i+1)}{\sqrt{i+2}}[-A(z)]^i$ are associated with the time average of the scattered light in SLIM, where $A(z) = \alpha_2 I_0 \int_0^z \frac{e^{-\alpha_1 z'}}{1 + \Delta z'^2/z_R^2}dz'$ (all details can be found in [28]). The subscripts S and A correspond to the scattering and absorption contributions for the extinction coefficient. Therefore, the NL extinction coefficient can be written as $\alpha_2 = \alpha_{2,S} + \alpha_{2,A}$.

To explicitly indicate the contribution of NL scattering to the extinction coefficient, a parameter S can be added in the form $\alpha_{2,S} = S\alpha_2$ and $\alpha_{2,A} = (1 - S)\alpha_2$. The expression allows defining if the NL extinction is entirely due to the NL scattering ($S = 1$) or to the NL absorption ($S = 0$). If the NL extinction is given only by NL absorption, $\alpha_{2,S} = 0$, and then the logarithm involving Σ_2 becomes zero. Thus, the term involving Σ_2 is a characteristic signature of NL scattering and can be used to distinguish between NL absorption and NL scattering contributions in the SLIM.

IV. RESULTS AND DISCUSSION

To discriminate the contributions of NL scattering from those of NL absorption, it is necessary to perform experimental measurements of the linear and NL extinction coefficients (using the OA Z-scan technique), as well as to characterize the laser parameters and beam longitudinal power profile by using SLIM. The sequence of measurements and analysis of the experimental results is described below.

A. Linear extinction coefficient

The samples provide a strong linear scattering at 532 nm because both TiO$_2$ and acetone are very transparent at this wavelength, and TiO$_2$-NPs present a large refractive index (e.g., $n_{NP} \approx 2.6$ at $\lambda = 632.8$ nm) compared with the acetone refractive index ($n_{solvent} = 1.36$) [31]. Thus the linear extinction coefficient in the samples is essentially the scattering, with negligible absorption contributions. This is evidenced experimentally by the fact that the scattering signal detected is quickly saturated by using the spectrometer. In this way, the linear extinction coefficients (α_1) for each sample (**A**, **B**, and **C**) reported in Table I, were determined by fitting the curves of lower incident intensity obtained by SLIM through Eq. (2).

B. Nonlinear refraction

As reported in [27], SLIM can be used to measure the nonlinear refractive index in scattering media (n_2) by monitoring the propagation of the incident laser beam within the sample.

TABLE I. Linear extinction coefficient (α_1) values of TiO$_2$-NPs suspended in acetone, obtained by SLIM at 532 nm, using Eq. (2).

Samples	**A**	**B**	**C**
α_1 (cm^{-1})	0.41	0.60	0.91

Since the measurement of n_2 depends on the sensitivity to analyze the beam divergence, the NL medium is placed so that its entrance face coincides with the focal plane of the focusing lens [see Fig. 1(a)]. Such optical setup ensures that the collected images show a clear contrast between the beam size at focus and far from focus, optimizing sensitivity in beam divergence analysis. However, under the experimental conditions used here, with the beam waist located at $z_0 = (2.6 \pm 0.1)$ mm within a 10-mm-thick cell, it was not possible to observe variations in beam divergence with increasing intensity (up to 12.5 GW/cm^2). Here the position of the beam waist within the sample was strategically chosen to measure the power variations of scattered light in regions around the focus, where NL effects are predominant due to high intensity and are not directly relevant for the NL scattering (as discussed in [28]).

C. Nonlinear extinction coefficient

Figure 3 shows the NL extinction curves obtained by the OA Z-scan technique for samples **A**, **B** and **C**, contained in thin cuvettes ($L = 1$ mm). The effective NL extinction coefficient can be found by fitting the expression $T(z) = \frac{1}{\sqrt{\pi} q_0(z,0)} \int_{-\infty}^{+\infty} \log[1 + q_0(z,0)e^{-\tau^2}] d\tau$ [22], where $q_0(z,t) = \frac{\alpha_2 I_0(t) L_{\text{eff}}}{1 + (\frac{z}{z_0})^2}$ and $L_{\text{eff}} = \frac{(1 - e^{-\alpha_1 L})}{\alpha_1}$. The decrease in transmittance around the focal position, $z = 0$, indicates that the NL extinction coefficient increases with the TiO$_2$-NPs concentration, as displayed in Table II. On the other hand, the standard deviation, obtained by five repeated measurements, decreased with an increased concentration of NPs. This is observed because the more intense the NL extinction effect, the better is the Z-scan sensitivity. In contrast, the more concentrated solutions exhibit larger fluctuations in the transmittance curve, as can be seen in the region furthest from $z = 0$, owing to the increase in the linear scattering strength due to a larger number of scattering NPs. The inset of Fig. 3 shows the normalized transmittance value in $z = 0$ (black solid circles) as a function of the volume fraction. Its linear fit (red dashed line) endorses
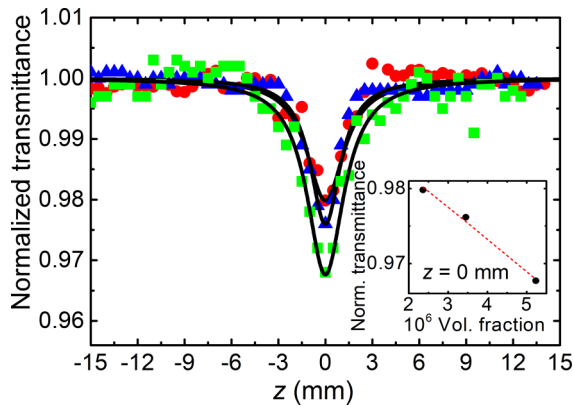

FIG. 3. OA Z-scan curves for samples **A** (red solid circles), **B** (blue solid triangles), and **C** (green solid squares) for $I_0 = 9.4$ GW/cm^2 showing the NL extinction effects. Inset: Normalized transmittance values at $z = 0$ mm (black solid circles) for each sample and with its linear fit (red dashed line) given by $y = 0.99 - 4.27 \times 10^3 x$, where x is the volume fraction.

TABLE II. NL extinction coefficients obtained by the OA Z-scan technique.

Samples	**A**	**B**	**C**
α_2 ($\times 10^{-11}$ cm/W)	6.3 ± 0.8	7.6 ± 0.7	10.2 ± 0.5

that the higher the TiO$_2$-NPs concentration, the higher the light NL extinction.

D. Nonlinear scattering characterization

1. Discrimination of the nonlinear scattering and nonlinear absorption

Figure 4 shows the natural logarithm of the beam power $\ln[P(z)]$ as a function of the z position into samples **A**, **B**, and **C**, for input irradiance between 2.5 and 12.5 GW/cm^2. The data obtained by using the SLIM were fitted by using Eq. (2). Notice that with the previous measurements, only C and S remain as free parameters for fitting, while the α_1 and α_2 coefficients were those presented in Tables I and II, respectively.

Notice, however, that the power of the scattered light contributing to the formation of the SLIM image should be reduced for positions beyond the focal point in the cell, since this contribution is spatially incoherent and diverges faster than the laser beam. Therefore, the model should be valid after the beam waist. Without loss of generality, it is possible to use the second half of the cell, i.e., the region between positions $z = 4$ and $z = 10$ mm in the cell, to fit the model described in Eq. (2).

The S parameter was studied by considering the previously measured parameters (beam parameters and NL extinction coefficient) and then determining the least average variance between the model and the experimental data for all measurements of a given sample. The average variance is the average value of the variance calculation between experimental and fitted data, for each corresponding z position. For all samples, the average variances in the range of $z = 4$ to 10 mm are shown for each value of S in Fig. 5. The values of S used in Eq. (2) to fit the experimental data of Fig. 4 correspond to the minimum value average variance of the curves presented in Fig. 5. Notice how the model adequately describes the data, except for the region of excess scattering close to the beam waist. Furthermore, since $0.7 \leqslant S \leqslant 0.9$ minimizes the average variance for all samples, it indicates that NL scattering is an important process that defines the nonlinear optical response of these samples.

Notice that the variances shown in Fig. 5 have a parabolic dependence on S. This is consistent with a Gaussian-like statistical process where S is the only free parameter and can be used to estimate the uncertainty over S. In particular, for a Gaussian process it is known that the curvature gives the inverse of the variance. Therefore, the curves shown in Fig. 5 were fitted by a parabolic function $F(x) = ax^2 + bx + c$, and the uncertainty over S is given by $\Delta S = \frac{1}{\sqrt{a}}$. This procedure was accomplished for each curve and S value and its respective uncertainty for each sample is presented in Table III.
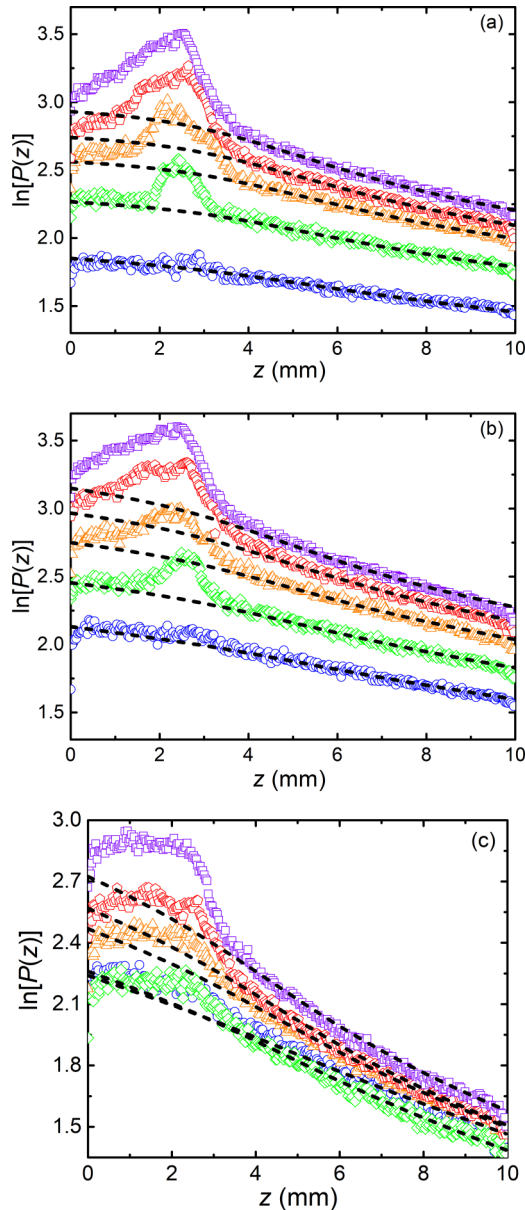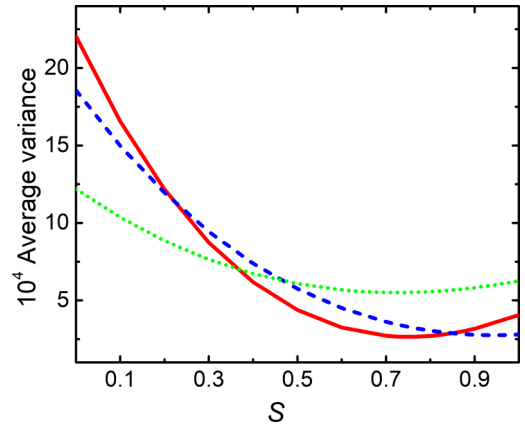
FIG. 5. Variance in the function of the S parameter for samples **A** (red solid line), **B** (blue dashed line), and **C** (green dotted line). The variance was calculated by SLIM experimental transmittance and fit data presented in Fig. 4. Each curve is an average of the average variance obtained for each one of five used I_0 values.

FIG. 4. Laser beam power as a function of z-propagation position (colored points) for samples (a) **A**, (b) **B**, and (c) **C** for five input beam irradiances (I_0) that vary from 2.5 (blue circles) to 12.5 (purple squares) GW/cm^2. The fitted curves (black dashed lines) were done with S equal to (a) 0.75, (b) 0.95, and (c) 0.72.

The values determined for the fraction of scattered light S are consistent among themselves (within the margin of error) for all samples and indicate a strong contribution due to NL scattering. In Fig. 5 and Table III one can see that the average variance versus S for sample **C** has systematically

TABLE III. S parameter of the samples calculated by the parabolic curve fitted in the results of Fig. 5.

Samples	**A**	**B**	**C**
S	0.7 ± 0.2	0.9 ± 0.2	0.7 ± 0.3

higher values and comprises a broader range of S values (uncertainty equals to 0.3) than samples **A** and **B** (both with 0.2 of uncertainty). Such uncertainty is a consequence of the α_2 coefficients that were determined from the Z-scan measurements, which presented standard deviations of $\pm 10\%$ (Table II). Hence, it is possible that a more precise determination of the NL extinction will lead to calculations of S with greater accuracy. It is worth mentioning that noise due to linear scattering is more relevant in sample **C**, since it contains more NPs. This situation requires an optical system with high sensitivity for making SLIM images. For this work only an 8 bit depth camera was available in the laboratory. But a camera with 10 bits or more should significantly improve the data collected near the end of the cell.

The images collected by SLIM show that most of the scattered power is observed in the first half of the cell, particularly around the beam waist region. As mentioned, this may be due to the contributions of the forward and backward scattered light. These contributions still need to be investigated, being the scope of future works. In addition, and reiterating, as the theoretical model contemplates the second half of the cell, where the beam has already diverged significantly, and the signal-to-noise ratio has degraded.

Next, we will consider two situations to illustrate the importance of SLIM and the model proposed in Sec. III to determine the NL scattering parameters of the samples. In the first case, it is assumed that the media exhibit linear extinction (with negligible nonlinear contributions), while in the second case, the contribution for NL extinction is considered to be due to pure NL absorption, as described below:

a. Linear regime case, $\alpha_2 = 0$. To illustrate this case, let us assume that the experimental results refer only to a linear regime. Figure 6 shows our results modeled by Eq. (2) considering only the linear parameters ($\alpha_2 = 0$). As can be seen, only the curves obtained for samples **A** and **B** at low intensity show agreement with the experimental results. This allows us to infer that at high intensities, the samples exhibit significant NL extinction behavior.
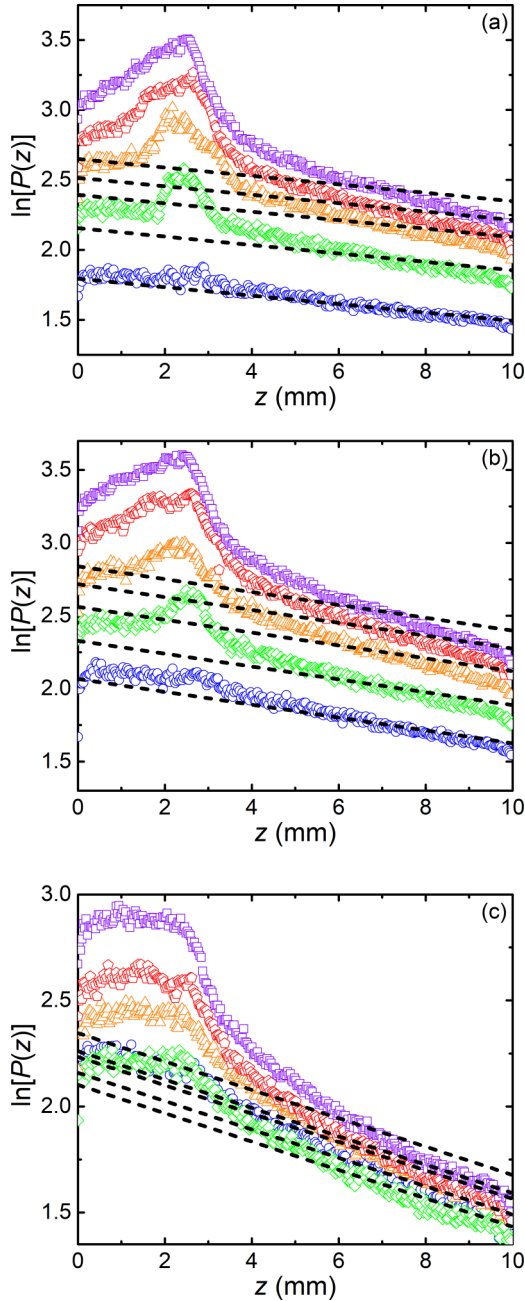
FIG. 6. Laser beam power as a function of *z*-propagation position (colored points) for samples (a) **A**, (b) **B**, and (c) **C** for five input beam irradiances (I_0) that vary from 2.5 (blue circles) to 12.5 (purple squares) GW/cm². The fitted curves (black dashed lines) were done with $\alpha_2 = 0$, only linear regime.

FIG. 7. Laser beam power as a function of *z*-propagation position (colored points) for samples (a) **A**, (b) **B**, and (c) **C** for five input beam irradiances (I_0) that vary from 2.5 (blue circles) to 12.5 (purple squares) GW/cm². The fitted curves (black dashed lines) were done with $S = 0$, taking on $\alpha_2 = \alpha_{2,A}$, only NL absorption.

b. NL regime case, only NL absorption ($S = 0$). Figure 7 shows the experimental data modeled from the theory described in Sec. III, considering $S = 0$, i.e., assuming that the NL scattering contribution is negligible. Notice that the theoretical curves are not consistent with the experimental data, which implies that the model considering only NL absorption is not adequate. This analysis also corroborates the variance analysis performed results obtained in Fig. 5 and Table III.

The inconsistencies between the theoretical curves and the experimental data shown in Figs. 6 and 7 reveal the impor-
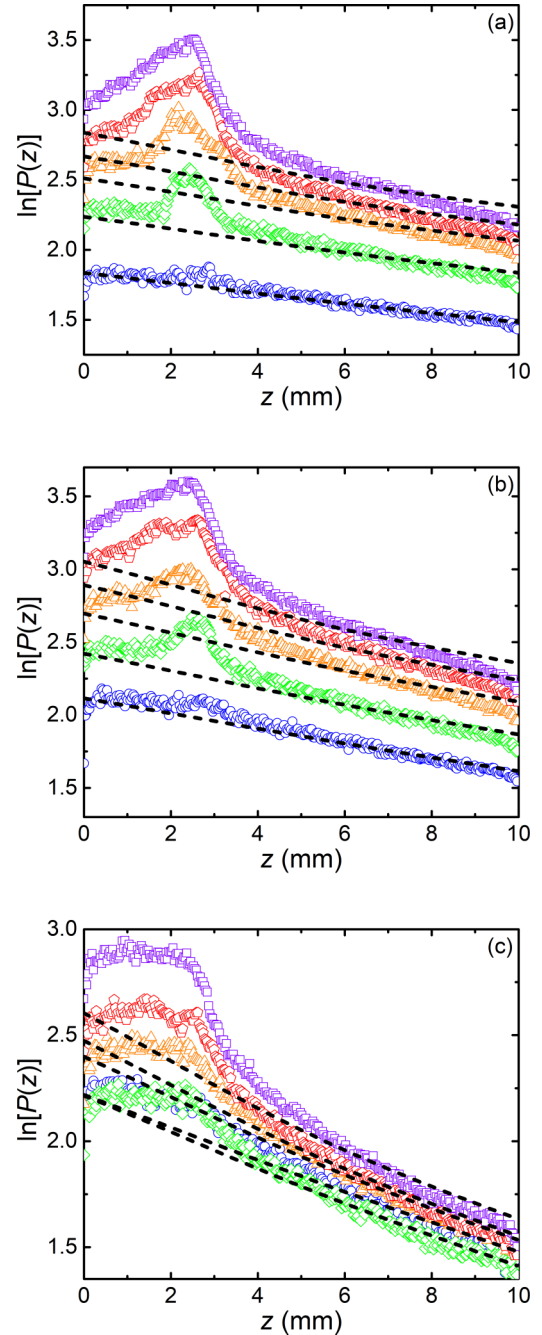
tance of NL scattering contributions for the light extinction behavior in samples containing TiO₂-NPs suspended in acetone.

2. Increased scattering near the waist

The behavior of the beam longitudinal power profile, shown in Fig. 4, reveals some unusual characteristics that need to be analyzed. Typically, in purely absorptive media, the beam power decreases exponentially upon propagation

through the sample. However, Fig. 4 displays an evident increase in the scattered power collected in the beam waist region (between $z = 0.0$ and 4.0 mm). Also, notice the increased scattering curve changes with the incident intensity. The maximum detected scattered power is located at $z = 2.6$ mm, precisely at the beam waist position (z_0) where the laser beam intensity is maximum. The explanation of the physical origin for the increase in scattered power requires a more refined model than the one considered in the present paper. For now, we hypothesize that this behavior is due to the forward and backward NL scattering contributions close to the beam waist. In the experiment, the backscattered light is again scattered by the nanoparticles, and therefore detected by SLIM. Mechanisms such as NL stimulated scattering can be induced in acetone, multiple NL scattering may be relevant for such small inclusions, and even intense pulse propagation processes such as filamentation can induce NL scattering [32–35]. For instance, the threshold power for filamentation in acetone is $P_{\text{Th}} = \frac{\pi(\lambda \times 0.61)^2}{8n_0 n_2} \cong 0.11$ MW [34], which corresponds to a critical intensity of $I_{\text{Th}} = \frac{P_{Th}}{\pi w_0^2} \cong 3.0$ GW/cm^2 in our case. This intensity is close to the smallest intensity used in our experiments, and the beam focus inside the sample facilitates the filament formation.

Figure 8 presents a brief analysis of this pronounced increase in scattered light from the subtraction between the experimental curve and its respective fitted curve in the region from right to left that begins at $z \approx 4.0$ mm and goes down to $z \approx 2.5$ mm extracted of each curve shown in Fig. 4. From that, the curves were fitted by $P_S(z) = \int I_S(z)dz = \frac{I_{S0}}{gI_L} \exp{(gI_L z)} = P_{S0} \exp{(gI_L z)}$, obtained by the integral of typical expression that governs an increasing curve due to the presence of stimulated scattering [32] given by $I_S(z) = I_{S0} \exp{(gI_L z)}$. In the previous expressions, $P_S(z)$ and $I_S(z)$ are the stimulated scattered power and intensity as a function of z-direction propagation, respectively, while I_{S0} and I_L are, respectively, the intensity at which the stimulated process begins and the intensity delivered by the laser. The values of the exponential argument in the equations above were found to be equal to $(gI_L z) \approx (2.0 \pm 0.3)z$, indicating that it could be a gain independent of the incident intensity value and much less dependent of the NPs density, and perhaps that the observed process is only due to the presence of acetone in all samples.

So, if we consider that acetone could be generating stimulated Brillouin scattering (SBS) assuming a Brillouin gain found in the literature $g_B = 12.9$ cm/GW at $\lambda = 532$ nm for this substance [33,34], we find that $(I_L g_B z) = (2.0 \pm 0.3)z \approx (0.015$ GW/mm$^2 \times 129$ mm/GW $\times z$ mm$)$, $I_L = (1.5 \pm 0.3)$ GW/cm^2, making it a possible situation for this experiment. The incident intensities of the laser beam are 2.5 to 12.5 GW/cm^2 and therefore, the strong scattering is observed from the power curves with incident intensity of 5.0 GW/cm^2. The increase in scattered power could be due to SBS. If this hypothesis is confirmed, this will indicate that backward scattering can be more than an optical phenomenon measured by SLIM in a single image, and so, to provide the scattered light measurement practically in all directions around the scattering plane. Therefore, the theoretical model does not describe the increased scattered light in this region, since the backscattered-light contribution is not included in the model.
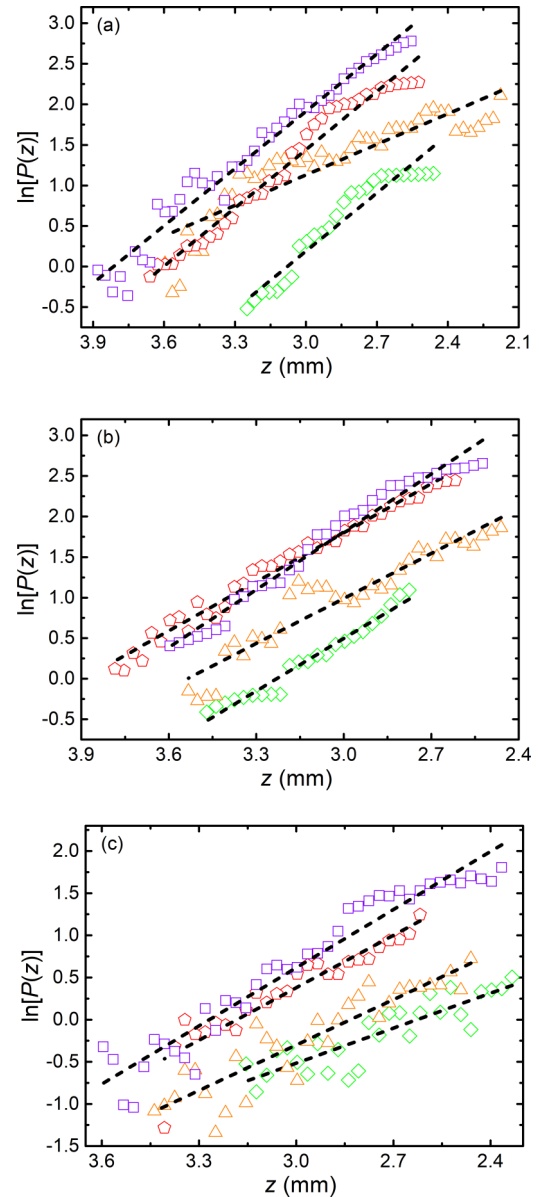

FIG. 8. Experimental natural logarithm of the scattered beam power curves minus the fit curves from our model in Eq. (2) as a function of the position along the propagation direction z (colored points) for samples (a) **A**, (b) **B**, and (c) **C**. In each figure, experimental data for four input beam irradiances I_0 are shown, being equal to 5.0 (green diamonds), 7.5 (orange triangles), 10.0 (red pentagons), and 12.5 (purple squares) GW/cm^2. Notice that the beam power grows exponentially towards the beginning of the sample (smaller z), which could be associated with a stimulated process along the backward direction. The fitted lines (black dashed lines) of each sample have average angular coefficient equal to (a) 2.1 ± 0.5; (b) 2.1 ± 0.2; and (c) 1.9 ± 0.3.

V. SUMMARY

In this work, the SLIM was used for complementary measurements to NL transmission experiments (OA Z-scan) to determine the ratio between NL scattering and NL absorption of turbid samples. As proof of principles, the NL extinction behavior of colloids consisting of TiO$_2$-NPs suspended in

acetone, with different concentrations, was studied. The analysis of the experimental results using the theoretical model described in [28] reveals that the NL scattering corresponds to $(80 \pm 20)\%$ of the total NL extinction coefficient. Therefore, SLIM can be considered an important tool to characterize NL extinction properties of turbid media since this technique can distinguish NL scattering contributions that are commonly attributed to NL absorption. The SLIM experimental setup allows us to perform the laser beam characterization (w_0, z_0, Z_R, θ, and M^2), record the laser beam power as a function of the propagation position in the sample [$P(z)$], determine the linear and NL extinction coefficients (α_1 and α_2), discriminate between NL scattering and NL absorption;

and maybe even the observation and determination of the scattered light in all directions, and the stimulated scattering gain (g).

[1] B. J. Berne and R. Pecora, *Dynamic Light Scattering: With Applications to Chemistry, Biology, and Physics* (Courier Corporation, North Chelmsford, MA, 2000).

[2] P. N. Prasad, *Introduction to Biophotonics* (John Wiley & Sons, New York, 2003).

[3] P. M. Carvalho, M. R. Felício, N. C. Santos, S. Gonçalves, and M. M. Domingues, Front. Chem. **6**, 237 (2018).

[4] S. K. Brar and M. Verma, TrAC Trends Anal. Chem. **30**, 4 (2011).

[5] K. C. Jorge, R. Riva, N. A. S. Rodrigues, and M. G. Destro, *Lasers in Manufacturing 2009 Proceedings of the Fifth International WLT-Conference Lasers in Manufacturing, Munich*, edited by A. Ostendorf, T. Graf, D. Petring, A. Otto, and W. G. Lasertechnik (AT-Fachverl, Germany, 2009), pp. 323–326.

[6] K. C. Jorge, R. Riva, N. A. Rodrigues, J. M. Sakamoto, and M. G. Destro, Appl. Opt. **53**, 4555 (2014).

[7] E. Kristensson, A. Ehn, J. Bood, and M. Aldén, Proc. Combustion Inst. **35**, 3689 (2015).

[8] A. Ehn, J. Zhu, X. Li, and J. Kiefer, Appl. Spectrosc. **71**, 341 (2017).

[9] C. J. S. de Matos, L. de S. Menezes, A. M. Brito-Silva, M. A. Martinez Gámez, A. S. L. Gomes, and C. B. de Araújo, Phys. Rev. Lett. **99**, 153903 (2007).

[10] B. Shivakiran Bhaktha, N. Bachelard, X. Noblin, and P. Sebbah, Appl. Phys. Lett. **101**, 151101 (2012).

[11] K. Jorge, M. Alvarado, E. Melo, M. Carreño, M. Alayo, and N. Wetter, Appl. Opt. **55**, 5393 (2016).

[12] A. Fratalocchi, G. Assanto, K. A. Brzdakiewicz, and M. A. Karpierz, Opt. Lett. **29**, 1530 (2004).

[13] A. S. Reyna, K. C. Jorge, and C. B. de Araújo, Phys. Rev. A **90**, 063835 (2014).

[14] A. S. Reyna and C. B. de Araújo, Opt. Lett. **41**, 191 (2016).

[15] A. S. Reyna, G. Boudebs, B. A. Malomed, and C. B. de Araújo, Phys. Rev. A **93**, 013840 (2016).

[16] R. Terhune, P. Maker, and C. Savage, Phys. Rev. Lett. **14**, 681 (1965).

[17] V. Joudrier, P. Bourdon, F. Hache, and C. Flytzanis, Appl. Phys. B **67**, 627 (1998).

[18] C. F. Bohren and D. R. Huffman, *Absorption and Scattering of Light by Small Particles* (Wiley, Berlin, 1998).

[19] N. T. C. Oliveira, A. S. Reyna, E. H. Falcão, and C. B. de Araújo, J. Phys. Chem. C **123**, 12997 (2019).

[20] H. C. Hulst and H. C. van de Hulst, *Light Scattering by Small Particles* (Courier Corporation, North Chelmsford, MA, 1981).

[21] M. Sheik-Bahae, A. A. Said, and E. W. Van Stryland, Opt. Lett. **14**, 955 (1989).

[22] M. Sheik-Bahae, A. A. Said, T.-H. Wei, D. J. Hagan, and E. W. Van Stryland, IEEE J. Quantum Electron. **26**, 760 (1990).

[23] N. Venkatram, D. N. Rao, and M. Akundi, Opt. Express **13**, 867 (2005).

[24] S. Kostritskii, M. Aillerie, E. Kokanyan, and O. Sevostyanov, Appl. Phys. B **125**, 160 (2019).

[25] M. R. Ferdinandus, M. Reichert, T. R. Ensley, H. Hu, D. A. Fishman, S. Webster, D. J. Hagan, and E. W. Van Stryland, Opt. Mater. Express **2**, 1776 (2012).

[26] P. Samineni, Z. Perret, W. S. Warren, and M. C. Fischer, Opt. Express **18**, 12727 (2010).

[27] K. C. Jorge, H. A. García, A. M. Amaral, A. S. Reyna, L. de S. Menezes, and C. B. de Araújo, Opt. Express **23**, 19512 (2015).

[28] A. M. Amaral, K. C. Jorge, C. B. de Araújo, and L. de S. Menezes, Phys. Rev. A **102**, 033503 (2020).

[29] I. Niskanen, V. Forsberg, D. Zakrisson, S. Reza, M. Hummelgård, B. Andres, I. Fedorov, T. Suopajärvi, H. Liimatainen, and G. Thungström, Chem. Eng. Sci. **201**, 222 (2019).

[30] ISO 11146-1, Standard, International Organization for Standardization, Geneva (2021).

[31] A. S. Gomes, A. L. Moura, C. B. de Araújo, and E. P. Raposo, Prog. Quantum Electron. **78**, 100343 (2021).

[32] D. Wang, R. Barille, and G. Rivoire, J. Opt. Soc. Am. B **14**, 2584 (1997).

[33] M. Bashkansky and J. Reintjes, in *Encyclopedia of Modern Optics*, edited by R. D. Guenther (Elsevier, Oxford, 2005), pp. 330–340.

[34] R. Boyd, *Nonlinear Optics* (Academic, New York, 2008).

[35] G. Boudebs, H. Wang, C. Cassagne, M. Chis, A. M. Amaral, and C. B. de Araújo, J. Opt. Soc. Am. B **36**, 3411 (2019).